NASA Technical Paper 3570

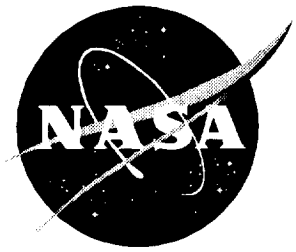

Performance Assessment of the Digital Array Scanned Interferometer (DASI) Concept

Stephen J. Katzberg and Richard B. Statham

August 1996

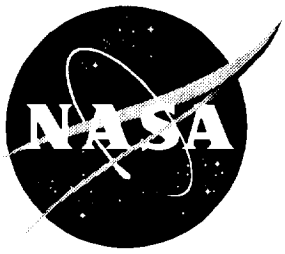

NASA Technical Paper 3570

Performance Assessment of the Digital Array Scanned Interferometer (DASI) Concept

Stephen J. Katzberg
Langley Research Center • Hampton, Virginia

Richard B. Statham
Lockheed Martin Engineering & Sciences Company • Hampton, Virginia

National Aeronautics and Space Administration
Langley Research Center • Hampton, Virginia 23681-0001

August 1996

Available electronically at the following URL address: http://techreports.larc.nasa.gov/ltrs/ltrs.html

Printed copies available from the following:

NASA Center for AeroSpace Information
800 Elkridge Landing Road
Linthicum Heights, MD 21090-2934
(301) 621-0390

National Technical Information Service (NTIS)
5285 Port Royal Road
Springfield, VA 22161-2171
(703) 487-4650

Contents

Symbols

A	area (e.g., of optics or gratings)
A_0	amplitude of plane wave $A_0 e^{ik'r'}$
a	entrance slit half-width
B	source brightness or spectral radiance
b	exit slit half-width
D	angular dispersion $d\theta/d\lambda$, variable source size
D_0	source size at upper limit of integral
D^*	$= (A\ \Delta f)^{1/2}/\text{NEP}$, normalized performance factor for detectors, cm $(\text{Hz})^{1/2}/\text{W}$
d	grating groove spacing, distance between mirror M1 and M2 images in y direction, source-apparent displacement distance in shearing two-beam interferometer
$d\mu$	wavelength interval in integral with change of variable in noise calculation
$d\sigma$	incremental wave number in integration
E	$= A_0 e^{ik'r'}$, field of plane wave
E_1, E_2	plane waves 1 and 2
e	exit
F	source-to-lens distance
$F(\sigma)$	detector transform factor in interferometer focal plane
f	lens focal length
I	$= (E_1 + E_2)(E_1 + E_2)^*$, intensity of the interferogram
$I_{(D_0, X_0, y)}$	intensity of source as function of D_0, X_0, and y
$I_{(x, y)}$	intensity of source in x-y coordinates of detector plane
i	entrance or initial
i_x, i_y, i_z	unit vectors in the x, y, and z directions
K	integral sum interval, a counter in interferogram inversion transform
$K_{\max}$	maximum summing interval in inversion of interferogram transform $K = 0$ to $K_{\max}$
k	scale factor normally a constant, sample number in digital interferogram inversion
k'	$2\pi\sigma$ term in plane wave $A_0 e^{ik'r'}$, alternate sample number in digital interferogram inversion
k_i	$= i\ \delta k$
$k_{\max}$	$= N\ \delta k$
L	mirror displacement, mirror path length
L	length along mirror M1 from apex of mirror M1 and image of M2 at M1
L_0	total length of a two-sided interferogram
l	path difference in interferometer
M1, M2	mirrors in Michelson interferometer
m	distance from mirror M2 (image) to defocus point DY
N	number of interferogram transform samples (nominally number of detectors and/or $K_{\max}$)
NEP	noise equivalent power
n	grating order of interference

n_0	noise charge of photodetector having noise proportional to its area
$\Re$	$= \sigma/\delta\sigma$, resolvance or resolving power
r'	distance vector of plane wave $A_0 e^{ik'r'}$
rect	rectangular function, Signal = 1 if $b< x >a$, 0 otherwise
S	area (e.g., grating) normal to the input flux
S_{avg}	average spectrum signal
S_0	constant-value spectral irradiance
SF	scale factor
S/N	signal-to-noise ratio
$S(K)$	detected signal (interferogram) for unit quantum efficiency and unit time
$S(x)$	detected signal over linear dimension
$S(\theta)$	detected signal over angular dimension
$S(\theta_e)$	exit signal
$S(\mu)$	original spectrum in change of variable noise calculation
$S(\sigma)$	input spectrum to spectrometer
$S'(\sigma)$	recovered spectrum from summed interferogram transform
$S(\sigma, \theta)$	input signal over wave number and angular extent
$\langle S_n^2(\sigma)\rangle$	variance of noise on recovered spectrum
$U_0(\sigma_0)$	monochromatic source signal with $\sigma_0 < \sigma_{max}$
X_0	detector plane array upper limit (one-sided) in integral
x	height or length from the origin in focal plane
α	slit angular extent in dispersive direction, aperture size of angular dimension, detector angular width
α_S	circularly symmetric acceptance half-angle
β	vertical slit angular extent, detector angular length
β_G	slit angular width for grating spectrometer
β_S	slit angular width for Sagnac interferometer
Δ	detector subtense angle
ΔX, ΔY	linear defocus error in X and Y directions for Michelson interferometer
ΔX_{sample}	the sample length along interferogram in detector plane, detector width, allowable defocus blur
$\Delta\lambda$	spectral wavelength interval
$\Delta\sigma$	spectral wave-number interval
$\Delta(\sigma)$	delta function around zero (dc) wave number
δk	the smallest interval for integral sum (in interferogram inversion)
$\delta\lambda$	limiting wavelength resolution
$\delta\sigma$	wave number resolution interval, $1/N\delta k$, sinc function half-width
Θ	tilt angle between mirrors M1 and M2 in Michelson interferometer
Θ_S	angular subtense for first zero of sinc function

Θ'	angle of source edge of plane wave exiting interferometer monochromator
θ	angle, rad
θ_e	exit angle
θ_i	entrance angle
θ_{max}	maximum acceptance half-angle for maximum phase angle, normally π
λ	spectral wavelength
μ	wavenumber in change of variable noise calculation
σ	spectral wave number, cm^{-1}
σ_{max}	maximum wavenumber in spectral band required
τ	optical system transmission
τ'	average transmission across one fringe half-cycle, $1/2\pi$
Φ	initial photon flux
Φ'	subsequent photon flux
ϕ	angle of incidence
Ψ	incident ray angle to normal of mirror M1
Ω	acceptance solid angle, sr
$\otimes$	convolution operator

Introduction

Over the past several years there has been a continuing discussion in the literature concerning the relative merits of dispersion-based (gratings, prisms, or other) spectrometers versus interference-based implementations. In general the interference-based instruments offer higher throughput than the grating instruments but have offsetting peculiarities, such as wavelength ambiguity or spectrum transform outputs.

An active dialog has existed both in and out of the literature between advocates claiming superiority for one or another technique. Recently, still another implementation of the interferometric technique has appeared. Called the digital array scanned interferometer (DASI) (refs. 1–4), the new technique is designed to make use of the interferometer advantages. (Earlier versions, developed or proposed, include the photodiode array Fourier transform spectrometer (PAFS) of ref. 5, and the interferometric diode array spectrometer (IDAS) of ref. 6.)

The DASI serves as the focus of this paper because it is a recent entry in the field of interferometer implementations and is claimed to have major benefits for certain NASA multispectral imaging applications. Although the claims for DASI have been presented in various ways, they can be grouped into three general categories with corollaries. The claims are that (1) DASI has a much higher étendue than grating spectrometers, (2) DASI's have an optimum instrument sampling function, and (3) DASI possesses several smaller systems-level capabilities. Some of the systems-level capabilities are the Fellgett (or multiplex) advantage, wavelength linearity, and well-known and easily correctable system errors, among others.

This paper reviews the operational principles of interferometric and dispersive spectrometers and presents the various claims for DASI. The paper assesses the DASI claims with respect to the operational principles presented to determine whether those claims can be substantiated. Finally, the results are summarized to serve as a guide to help determine what role DASI's might play in appropriate applications.

Overview of Spectrometer Principles and Characteristics

A monochromator or spectrometer takes selected incoming radiation and spatially disperses that radiation into spectral components that can be individually identified. This process can be accomplished in several ways, but the most common methods are broadband filters, direct measurement by means of wavelength dispersion, and indirect measurement by some transformation process. This paper addresses only the dispersion and transformation techniques. The material in this development depends heavily on that of Jacquinot (ref. 7).

Luminosity, Étendue, and Resolving Power

Of importance to any spectrometer implementation are the resolving power and the luminosity. Resolving power (or *resolvance*) is given by $\Re = \lambda/\Delta\lambda$, and luminosity is given by the ratio of the detected power to the available power for that measurement.

For luminosity, the governing parameter is the *étendue*, which represents the size and angular constraints on the amount of energy an optical system can pass. Étendue is given by the product $A\Omega$, where A is the area of the optical aperture and Ω is the solid acceptance angle of the same optics. This equation is simply a direct consequence of the conservation of energy in an optical system: $\Phi = B\tau A\Omega$. In this equation, B represents the brightness, or spectral radiance, of the source, and τ represents the system transmission. Furthermore, $\Phi' < \Phi$, where Φ' is the flux of subsequent optical stages.

The desired goal is to have maximum flux at maximum resolving power. However, there is usually a trade-off between resolving power and angular acceptance. One often must sacrifice resolution to achieve higher signal throughput.

Grating Spectrometers

Dispersion spectrometers have two general implementations: prism and grating. In either case, a spectrum is determined by illuminating a slit by some source, passing the light through the prism, or reflecting or transmitting the light via a grating. The resulting light then illuminates an exit slit, detector, or detector array. In most prism and grating systems, the entrance slit is imaged onto the exit slit or detector array by the collimating and imaging optics with allowance for any required scale adjustment.

For the prism, the light is refracted differently as a function of wavelength, giving different exit angles. A detector or slit, defining an exit angular subtense, receives energy from a restricted wavelength range. Changing the slit location or detector location in some uniform way yields a spectrum whose resolution depends on the entrance and exit slit widths. The prism fails to perform its function as its index ceases to have a variation with wavelength, a case for many transparent materials at long wavelength. Available signal-to-noise ratio depends on the amount of energy at the detector, with decreasing slit widths yielding reduced energy. Resolution, on the other hand, increases with decreasing slit widths, giving the fundamental trade-off of signal-to-noise ratio versus spectral resolution. Because

the prism generally is considered inferior to the grating, it will not be considered further.

The grating spectrometer, illustrated in figure 1, appears similar to the prism in implementation, but operates by means of an entirely different principle. The dispersion in a grating comes from an interference effect generated by reflection from a parallel pattern of grooves or refraction from a pattern of index modulation in transmission.

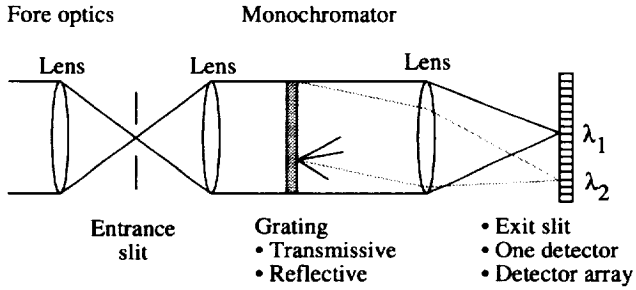

Figure 1. Grating spectrometer.

For the more efficient and common reflection grating, the condition between the incidence angle and the exit angle that yields constructive interference is

$$d \sin\theta_i \pm d \sin\theta_e = n\lambda$$

where d is the groove spacing, λ is the wavelength, θ_i represents the entrance angle, θ_e represents the exit angle, and n represents the order of the interference. The order of the dispersion refers to the fact that the grating can give constructive interference as long as the path lengths are in integral multiples of one wavelength. Typically, the first order is the strongest, but by "blazing" the grating, either certain wavelengths or orders can be enhanced. Notice that half the wavelength at the second order gives the same constructive interference and conditions on angles as the first order. Gratings, therefore, require bandpass filters, "order-sorters," that limit the incoming wavelengths to some broad band without the possibility of higher orders coming through. Detectors with specific spectral ranges sometimes can eliminate the need for order-sorters.

As with the prism, the grating spectrometer images the entrance slit onto the exit slit or onto a detector (array). In the case of the exit slit, moving the slit so that it covers the range of angles required generates a spectrum. Rotating the grating gives the same effect. A detector array simultaneously samples the entire spectrum, if the array is large enough.

Again, as with the prism, a combination effect of the entrance slit angular width and that of the exit slit or detector element sets the resolution. The spectral resolution increases with decreasing slit or detector widths, while the energy detected goes down, again, in a fashion similar to that of the prism.

It is important to note that the effect of the slits (or slit and detector aperture) can be modeled in the following way. Given a monochromatic source filling the entrance slit, the optics form an image of the slit at a location on the exit image plane consistent with the grating equation shown previously. As an exit slit is scanned across the image, a detector first records a signal that increases, perhaps stays constant for a bit, and then drops off to zero. Analytically this signal pattern equals the convolution $\otimes$ (ignoring the effects of imperfect optics):

$$S(\theta_e) = \text{rect}(k\theta_i/a) \otimes \text{rect}(\theta_e/b)$$

where $S(\theta_e)$ is the exit signal, a represents the half-width of the entrance slit, b represents the exit slit half-width, and k represents any scale factor between the entrance and exit optics.

The case differs slightly for a detector array. The detector array represents a set of spatial or angular samples, and if the detectors are fine enough, an output similar to the exit slit is obtained. Imagine that the detector signals are read in groups whose total angular subtense equals that of the exit slit already discussed. Imagine further that a spectrum is developed by moving along the detector array one detector at a time. This method is equivalent to using the exit slit with tiny, but discrete steps. Clearly the two cases yield similar results. In addition, from reference 7, the maximum resolution-energy product occurs for exit and entrance slits (or images) that are matched.

The effect of a polychromatic source is then a convolution of the monochromatic exit response with the source spectral distribution, all referenced to the exit region. It is very important to note that any *spatial* variability in the entrance slit is transformed to the exit slit according to the spectral content. In addition, a *grating has dispersion only in the one dimension,* while along the nondispersive direction the grating acts as a mirror.

As stated by Jacquinot (ref. 7), the relationship between energy throughput and resolution for a grating monochromator can be developed as follows. Matching the spectral width of the input and exit dispersions α_1/D_1 and α_2/D_2 (where $D = d\theta/d\lambda$) yields the highest throughput. Given this condition, the limiting resolution $\delta\lambda$ of

the monochromator is α_2/D_2 (= α_1/D_1). The maximum flux being detected is then

$$\Phi = \tau BS\Omega$$

where S is the area of the grating normal to the input flux, B is the source spectral radiance, τ is transmission, and Ω is the solid acceptance angle at the grating.

Alternatively, with the value β representing the vertical slit angular extent and α_2 representing the dispersive direction angular extent,

$$\Phi = \tau BS\alpha_2\beta$$

$$\Phi = \tau BS\lambda\beta D_2/\Re$$

where resolving power is given by $\Re = \lambda/\delta\lambda$. This result says that output flux is inversely proportional to resolving power, expressing analytically what was alluded to earlier.

In a typical case of a high-throughput system, e.g., a Littrow mounting, $SD_2 = (2A \sin\phi)/\lambda$, where A is the area of grating and ϕ is angle in incidence. This allows the final result

$$\Phi = \tau B2A\beta(\sin\phi)/\Re$$

For the grating with fixed resolution and collimating optics diameter, increased energy throughput can only come by increasing the slit size in the nondispersion direction. Jacquinot states: "Practical limitations restrict the acceptance angle β to about 0.1 radian" (ref. 7). More modern system designs may improve on this value, but the conclusion is still valid as a practical baseline.

Interferometers

To compare the performance of the current DASI interferometers with their grating competitors, one must start somewhere near the beginning of interferometers as instruments, e.g., the Michelson interferometer, and then move on to the variations leading to the DASI. The material here follows reference 8.

In certain situations, it is possible to see interference fringes from nearly monochromatic light, and in some cases, white light over restricted ranges. It is difficult to achieve fringes from broadband light for the simple reason that broadband light, though intense enough, represents a linear superposition of interference from many spectral bands that hopelessly overlap and wash out the fringes. Moreover, light arising from different areas of the source is uncorrelated, so increasing the source size does not usually intensify the fringes. Making the light quasi-monochromatic enough by reducing the bandwidth by filtering results in a lack of sufficient light in the wave band of interest. If extended sources are used to increase the available light, existing fringes are generally "washed out" because the extended sources cause overlap of the fringes. Fringes may still be visible, but they may become localized.

If a partially reflecting mirror and set of reflecting mirrors are arranged so that light passes in two different legs (fig. 2), one or both of which have adjustable path lengths, the result is the Michelson interferometer. The partially reflecting mirror divides the light into two (equal) amplitude components, each of which recombines with itself at some exit plane. Following the path from any point on an extended source for the Michelson, one finds fringes formed by the interference of all parallel rays from all parts of the source. The apparent location of these fringes is at infinity. In reality the fringes form behind a lens focused at infinity. Because each bundle of rays from the source splits in two and all rays that are parallel to one another come to a focus together, yielding what are called "fringes of equal inclination," they are said to be "localized at infinity." All regions have matched ray pairs regardless of the size of the source. Thus, the Michelson interferometers, and some relatives, have the characteristic of their fringe *visibility* being unaffected by sensible source size extension. The intensity of the fringes goes up, while their contrast remains high.

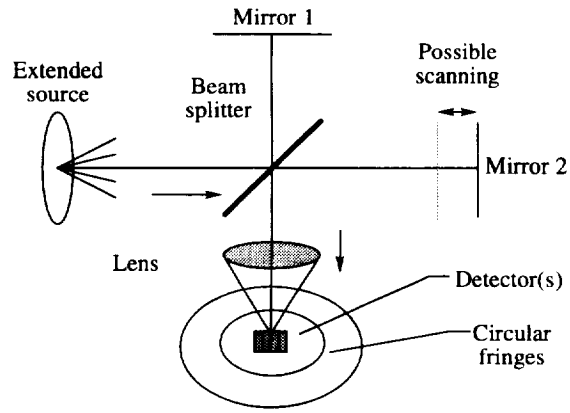

Figure 2. Michelson interferometer.

The Michelson operates by having one of its plates displaced so that the distance traversed in one leg is longer than the other. Fringes for the Michelson take the form of concentric rings whose spacing varies inversely as the square of the angle from the central fringe or ring. As the distance in one leg varies, the fringes contract or expand from the center.

Placing a detector at the fringe center, illuminating the interferometer with narrow band radiation, and

varying the path length differential in some linear fashion with time yields a sinusoidal pattern. Polychromatic radiation yields a linear sum of sinusoids whose period is determined by wavelength and path length difference. The overall effect is to generate a cosine Fourier transform of the source spectral content linear in wave number. Note that out along the fringe plane (in the focal plane of the lens) the same Fourier transform exists, although with a nonlinear scale. The Michelson interferometer, with its ability to accept large source sizes, has a considerable advantage as a nonimaging spectrometer, as will be seen later.

Important Result: Note carefully that the corollary to the wide acceptance angle for fringes of equal inclination in the Michelson is the loss of spatial information. With the exception of a source at a great distance, all parts of the source are distributed uniformly in the rings, and spatial detail is lost.

Another property of the Michelson is important in understanding the DASI. If the mirrors on the Michelson are set at zero differential path length, but cocked at a small angle, the fringes become nearly parallel and are aligned along the apex of the virtual air wedge formed by the two mirrors.

If the Michelson is carried one step farther, an interferometer that has linear fringes can be formed (the Sagnac interferometer illustrated in fig. 3). In the Sagnac, there is a beam splitter as before; however, the divided light is directed not back at the beam splitters from which it came but to the twin mirror in the interferometer. This configuration causes the resultant twin rays to traverse nearly the same path but to be displaced laterally. Thus, the light appears to come from two laterally displaced parallel sources to yield fringes of equal inclination localized at infinity. However, unlike the Michelson, the Sagnac fringes are parallel lines and not concentric annuli. Like the Michelson, the Sagnac has high fringe visibility with extended sources.

Moving one of the plates in or out from some point of approximately equal distance generates a Fourier transform in the Sagnac. A monochromatic source would produce a linear fringe pattern or, in a detector moving across the pattern, a sinusoidal signal dependent on the wavelength of the source and the movement of the plates:

$$S(x) = \int S(\sigma)\{1 + \cos[2\pi(\sin\theta)\sigma L]\}d\sigma$$

$$S(x) = \int S(\sigma)[1 + \cos(2\pi x\sigma L/f)]d\sigma$$

where $S(x)$ is the detected signal, L is $\sqrt{2}$ times the mirror displacement, θ is the lens incidence angle, f is the lens focal length, x is the distance in the focal plane, and σ is the wave number. Other than the constant term, the

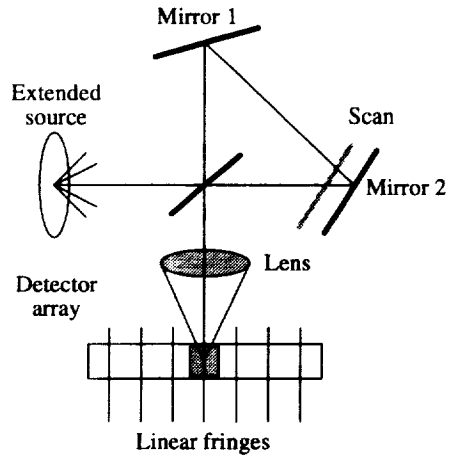

Figure 3. Sagnac interferometer.

detected signal is then proportional to the cosine transform of the source spectral distribution.

For the Sagnac and some other interferometers with parallel fringes, it is obvious that a detector array could sample the fringes. With the inherent transform scale linearity of the Sagnac-type implementations, interpretation would be simplified with respect to a Michelson.

A worthwhile digression here considers the two alternative implementations for Michelsons, Sagnacs, and others. Material presented earlier noted that Michelsons could have sources of large extent without reducing fringe visibility. When operated in this fashion, the fringes are localized at infinity and distributed over a plane behind a lens focused at infinity. An alternative implementation, the Twyman-Green interferometer in figure 4, results when the Michelson is illuminated by a collimated source of finite, but small, angular subtense. In this case the annular fringes are compressed into a region set by the angular subtense of the source size. An interference pattern is generated by moving the plates and observing the detector output. The latter case is appropriate for a single detector, whereas the extended source case would be appropriate for a detector array of concentric annuli. In both cases, the mirror plates of the interferometers generate fringes that appear to be localized at infinity. If the plates of the interferometers are close to zero displacement and cocked to generate nonparallel exit rays, the fringes become localized in the virtual wedge formed by the mirrors.

The relationship quantifying interferometer resolution and throughput can be found by following Jacquinot (ref. 7). Two cases are noted, one developed by Jacquinot in reference 7 and one by Vanasse and Sakai (ref. 9). Both are related and important to DASI. Jacquinot based his resolution argument on a Fabry-Perot etalon, with

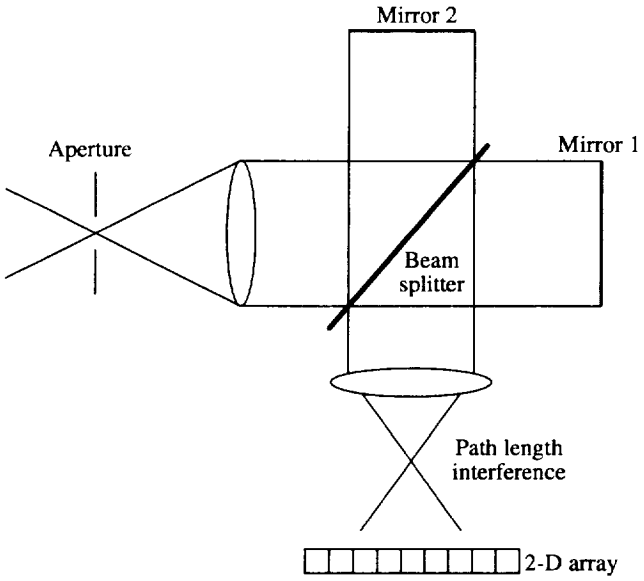

Figure 4. Twyman-Green interferometer.

further discussion in reference 7. He did not present a direct analysis applicable to the DASI case. Vanasse and Sakai discuss the finite aperture case for the collimated Michelson (Twyman-Green) interferometer and developed the following result. Given the circularly symmetric acceptance half-angle α_S, the relationship to resolvance $\Re$ can be written (ref. 9) as

$$2\alpha_S = \sqrt{(8/\Re)}$$

Noting that Ω is $\pi\alpha_S^2$, the relationship becomes

$$\Omega = 2\pi/\Re$$

This analysis is based on the fact that, as the incident light is allowed to move off axis by an extended source, a phase shift develops that is dependent quadratically on the off-axis angle. Setting this developing phase shift equal to $\pi/2$ gives the desired relationship. The relationship between resolution and solid angle expresses analytically the advantages of interferometers. Because étendue is set by the entrance pupil, usually some telescope in our case, it is of great advantage to have the spectrometer match the étendue of the front optics. For mirrors and lenses, the étendue of optics viewing an extended source can be much larger than that which is compatible with a grating monochromator. The prism monochromator is even less capable than the grating system. This front-end optics and monochromator mismatch presents less of a problem for point sources below the resolution limit for the front-end optics because the étendue is forced to be small.

Important Result: Both angular dimensions of the interferometer entrance solid angle can contribute energy to the interferogram. On the other hand, the spectral resolution reduces only weakly from the angular subtense. As shown for the grating monochromator, one angular dimension trades resolution directly for greater angular acceptance. The other dimension (β in the grating equation) can be increased only to a value of about 0.1 rad. Thus, the throughput advantage of interferometers over gratings is approximately $3.4/\beta$ (ref. 1), or about 34 for the best grating monochromators.

When required to perform as both spectrometer and imager, the interferometer must sacrifice some of its étendue advantage, as described in the following.

Parallel fringes, such as those caused by a thin air wedge, appear to come from areas of equal optical thickness and are called "fringes of equal thickness." The terminology "fringes of equal thickness" appears to originate from Fizeau fringes or Michelsons with inclination in the mirrors. In the Sagnac, fringes do not arise from contours of equal thickness but from laterally displaced beams or sheared source images whose differential path length varies with angle.

Resolution reduction in the Sagnac comes in a related though significantly different fashion from that in the Michelson. Any detector that spans a significant part of a fringe yields a signal with reduced modulation. Resolution reduction affects a particular wave number and those above, whereas lower wave numbers are less affected. Thus, in this case as well as for the Michelson, resolution reduction is less clear-cut in interpretation than might be desired.

The Sagnac also has an acceptance angle effect that yields blurring in the interferogram similar to that arising from a finite detector size (as shown in appendix A). The effect comes from the fixed lateral displacement of the two apparent sources in the presence of increasing acceptance angle for a Sagnac with the source near the optics focal point. In the Twyman-Green case, a similar effect occurs coupled with a defect of focus impact that can limit performance. Taken together, either the detector size or acceptance angle geometric effects yield an equivalent inverse resolvance versus (linear) acceptance angle trade-off. Reducing detector size only increases resolvance (without regard to signal-to-noise considerations) up to the point where the blurring effects predominate.

In system modeling terms, the resolution reduction corresponds to multiplying the reconstructed source spectrum by a term of the form $(\sin x)/x$ (sinc function) whose first zero is set by the reciprocal of the angular subtense of the detector or angular blurring combination,

whichever comes first. As shown in appendix A, the sinc function corresponding to a finite aperture size of angular dimension α causes the reconstructed spectrum to be multiplied by a sinc function whose first zero occurs at $\sigma = 1/l\alpha$, where l is the path difference.

For interferometers, the maximum modulation frequency sets the ultimate resolution in the transform process. This maximum modulation, in turn, comes from the maximum phase differential. The reconstructed transform is convolved with (smoothed by) a sinc function whose half-width is $\delta\sigma = 1/l\ \theta_{max}$.

Therefore, the resolvance can be written as

$$\Re = \sigma/\delta\sigma = 2\theta_{max}/\alpha \leq 2\pi/\alpha$$

where the maximum resolution is limited by the total possible acceptance half-angle π. Note the result is similar to that of the Michelson except the angle is not the *solid* angle subtended by the detector or other spatial integrating effect.

Important Result: For the Sagnac and similar interferometers, the spectral resolution is *not* inversely related to the acceptance solid angle. Rather, the resolution is inversely related to a single-dimension angle only. Therefore, the étendue for a square pixel $A\Omega$ is inversely proportional to the resolution squared—a very different result from that of the Michelson interferometer.

DASI Implementations

As noted earlier, linear fringe interferometers using detector arrays existed before the current DASI version (refs. 5 and 6). The common element in the implementations consists of some interferometer form that yields linear fringes plus a linear detector array. Thumbnail descriptions of some representative DASI versions that have been proposed follow.

Figure 3 shows a Sagnac form of DASI in which the light traverses a common path after being amplitude divided at a beam splitter. If the mirrors are set at unequal distances from the beam splitter, two laterally separated apparent sources arise. The apparent sources produce linear fringes at the back focal plane of the imaging lens; therefore, they are said to be "localized at infinity." There is no limitation perpendicular to the detector array except the size of the beam splitter lens-mirror combinations.

Another implementation of a DASI, illustrated in figure 5, uses birefringent prisms. Several versions utilizing birefringence are possible, but all are similar to the one using the Wollaston prism. In the Wollaston form, light is collimated from a source and passes to a prism made of two pieces of crossed birefringent material. Ordinary (o) and extraordinary (e) rays are split by a small angle in the prism. The rays are split across the entire height of the prism, with the effective path length difference between the rays approximately linearly related to a position along the height of the prism. The rays appear to be "localized" in the prism near the interface between the two halves. The rays are brought to a focus by a second lens with the linear detector array in the focal plane. Cylindrical lenses can be used to condense the parallel fringes onto the array for better signal-to-noise-ratio.

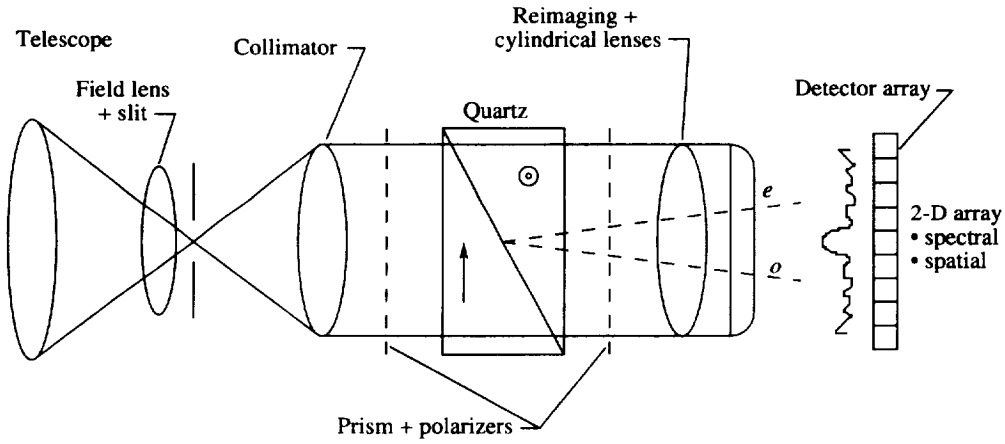

Figure 5. DASI with Wollaston prism configuration.

Table I. Various Claims of Performance Advantages for the DASI System

1. Much higher étendue for equal resolution (ref. 2, p. 5)
   10×–100× greater signal to noise at equal field of view (ref. 1, p. 418)
   Transmits more than 1000× more photons at same resolution and equal apertures (ref. 2, p. 5)
   Étendue greater than 1000× at given spectral resolution and equal aperture (ref. 2, pp. 5 and 10)
   Corollary: Can trade étendue for more compact size? (ref. 2, p. 10; ref. 3, p. 2).
   Corollary: Field-widened versions have accentuated advantages (ref. 2, p. 5; ref. 1, p. 421).

2. Data has optimum sinc instrument sampling function (ref. 1, p. 419).
   Frequency response is a rectangle (ref. 2, p. 5).
   Corollary: DASI has 3× resolution factor or more (ref. 2, p. 6).
   Corollary: Due to 3× resolution and sinc function, one-third the number of samples are required (ref. 2, p. 10).
   Corollary: Due to one-third samples, DASI achieves high signal to noise or higher resolution for same data volume (ref. 2, p. 10).

3. Miscellaneous systems level advantages
   System errors are known and correctable (ref. 2, p. 11)
   Superior linearity, throughput, dynamic range, spectral range, and fidelity (ref. 3, p. 2)
   Can use heterodyning (ref. 1, p. 419)
   Constant (wavelength) efficiency (ref. 1, p. 419)
   Transient event detection capability (ref. 2, p. 9)
   Multiplex advantage (ref. 2, p. 2)

DASI Claims

The collected literature, published and unpublished for DASI (refs. 1–4), has been surveyed for the claims made for DASI. Because there is considerable repetition, the claims have been collected into three main groups that capture their essence (table I).

Three major claims can be summarized as follows: (1) more throughput for a given resolution, (2) a better system response function, and (3) more benign system characteristics, including the multiplex advantage.

Claim 1—Higher Étendue

Claim 1 refers to the known fact that higher étendue is available in Michelson interferometers when compared with grating spectrometers. As noted earlier, Jacquinot (ref. 7) developed a comparison between Fabry-Perots (F-P) and grating monochromators that showed that the ratio in throughput could be expressed as

$$\text{F-P/grating} \approx 3.4/\beta$$

References 9 and 10 further show that this result also holds for interferometers, such as Michelsons and others that generate annular fringes, as well as for Fabry-Perots.

In an implementation that takes advantage of the properties of interferometers or gratings, the design would attempt to set the instantaneous field of view (IFOV) with some foreoptics and utilize the largest mirror or lens that is compatible with practicality constraints. Because the étendue is constant, a small IFOV could be converted by magnification to something compatible with the resolution of the interferometer. Magnification reduces the area required in the interferometer or grating and increases the IFOV. Because resolvances of at least several tens or a few hundreds would be employed, the angular subtense would be from one to a few tenths of a radian, consistent with considerable scaling gain. Large-diameter foreoptics with small IFOV's are natural companions to smaller area spectrometers with moderate spectral resolution. For matched areas and resolutions, the interferometer offers approximately 30 times the throughput of the grating. The increased throughput can be used to increase the signal-to-noise ratio, to reduce size, or for a combination of both. (It should be noted here that in the photon-noise-limited applications usually addressed in the literature, the signal-to-noise gain from the throughput advantage would be around 5.5.) Linear dimension gains will be far less impressive in photon-noise-limited cases. Still, the diameter of the grating system would have to be 5.5 times greater than that for the interferometer in the photon noise case.

As shown in appendix A for Sagnacs (or Twyman-Greens with wedged mirrors) producing parallel fringes, the relationship between resolving power $\Re$ and acceptance angle is different from the Michelson case. Either the size of the detector angular subtense or the fringe contrast reduction from increased acceptance angle "blurring" causes a reciprocal relationship of the resolvance and acceptance angle. This is quite a different case from the Michelson or Twyman-Green case with parallel plates. Moreover, as shown in appendix A, there are additional effects from defocus on the higher spatial

frequency components of the transform for the Michelson and Twyman-Green. The Wollaston version case is similar when one realizes that the Wollaston is equivalent in a systems sense to a Twyman-Green with wedged mirrors.

Given these considerations, the ratio of Sagnac interferometer to grating monochromator detected power can be written:

$$\text{Sagnac/grating} \approx (2\pi\tau' BA\beta_S/\Re)(BA\tau\beta_G/\Re)$$

where τ' is the average transmission across one fringe half-cycle, equal to $1/2\pi$, and the factor 2 takes into account that the peak modulation is only 1/2. For the grating, following reference 7, a Littrow mounting and a blaze angle of 30° are assumed. However, when the β dimension must be allocated to spatial resolution, both angular subtends will be set by the required spatial resolution and will, therefore, be limited by optical quality considerations. The Michelson with annular fringes has an acceptance angle advantage at the cost of spatial information. The parallel-fringe DASI family gains the spatial dimension at the cost of reductions in the acceptance angle advantage. Put another way, when the interferometer must perform spatial imaging, it must sacrifice part of its superiority over the grating monochromator. Therefore, any comparison between interferometers and gratings used in spectrometer and imaging mode must compare compatible instruments.

The final result may be stated as follows: The parallel-fringe Sagnac-like interferometers are better than the grating only in the ratio of their respective "nonspectral resolution" angular subtends. Using this acceptance angle advantage for Michelsons (ref. 4) in forming comparisons, as has been done for DASI (refs. 1–4), amounts to comparing apples and oranges.

Claim 2—Optimum Sinc Function

The claim that DASI's frequency response is a rectangle comes from the fact that all components of the Fourier transform at the detector are weighted equally. In Fourier transform terms, systems that do not exactly replicate the input have system responses that are functions which modify the signal Fourier components. The weightings on the components for real systems tend to decrease with larger frequency values of the transform variable. A constant weighting, or "flat" frequency response, is equivalent to convolving the input function with a sinc function whose width is inversely proportional to the highest value of the frequency. This effect was discussed in the interferometer section. The greater the value of the highest Fourier component, the less smoothing of the data is required and the more detail is available.

Whereas reproducing fine detail is important, the instrument sinc function, which is not very well behaved, exhibits the Gibbs phenomenon, or "ringing." Thus, the high-resolution benefit of having a flat response is balanced by the danger of generating false detail. In practice, many interferometer spectrometers utilize apodization windows to avoid the ringing and consequent undesirable false detail (ref. 9).

The need to apodize reduces the flat response to one that attenuates the high-frequency detail in just the same fashion that the triangular response of a grating monochromator smoothes the direct spectrum. A typical apodization profile is a triangular ramp that goes to zero at the maximum frequency and is normally applied in postprocessing of the data. *As a result, DASI's (as well as other Fourier transform spectrometers) realize the "flat frequency response" at the expense of potentially erroneous spectrum interpretation.*

Claim 3—Multiplex and Other Advantages

This claim includes several smaller elements and one that appears to be a major claim—the multiplex advantage. Note that in the DASI references the multiplex advantage was also presented as a multiplex *disadvantage.* To see how this might be so, one must first understand the origin of the multiplex advantage.

Grating or prism spectrometers sample the spectrum directly with a noise measurement at each sample point–time interval. Fourier transform spectrometers, on the other hand, observe a linear sum of elements of all portions of the input spectrum. When reconstructed, the presumably uncorrelated noise samples combine incoherently, while the signal adds coherently. This result is commonly referred to as the Fellgett, or multiplex, advantage (ref. 11).

With early detectors and with some modern detectors in certain wavelength regions, detector and amplifier noise represent the major noise contamination of the signal. For some time, quantum-noise-limited photomultipliers were restricted to the visible and ultraviolet region of the spectrum. In the case of detector noise independent of the incoming signal, there is a multiplex advantage.

For modern detectors, such as silicon charge coupled devices (CCD's), HgCdTe-CCD hybrids, and others, the detector noise is commonly quantum-noise-like, depending on the square root of the detected photocurrent. Under these conditions, Kahn (ref. 12) has shown that the multiplex advantage disappears to be replaced by a noise dependence on wave number that is different between the interferometer and the grating spectrometer.

Kahn showed that the signal-to-noise ratio for an interferometer, when compared with a sequential grating monochromator in photon-noise-limited operation, favors the interferometer in spectral regions where the spectral content is more than twice the average spectral intensity. Modern technological implementations give the grating monochromator an advantage if a detector array is used in lieu of a rotating grating or movable detector. The detector array makes possible a signal-to-noise increase equal to the square root of the number of spectral samples and gives a multichannel advantage analogous to the multiplex advantage. With both the DASI and the grating monochromator taking advantage of detector arrays, the results of Kahn clearly apply equally to the nonmechanically scanned multiple detector case. Appendix B presents the sampled data version of the analysis in Kahn for the cases of monochromatic, narrowband, and broadband sources, as well as for photon-noise- and detector-noise-limited conditions. As shown in appendix B, this redistribution can have some beneficial effects, depending on the type of spectrum (lines or continuum) being observed. Single monochromatic lines yield a high signal-to-noise ratio with noise redistributed throughout the reconstructed spectrum. *For this case, were it not for other limitations described in appendix A, as well as in this text, the resolvance would continue to increase with increasing numbers of detectors without loss of signal-to-noise ratio.* For multiple monochromatic sources, the redistribution of the noise punishes the signal-to-noise ratio for the weaker lines.

For the case of broadband sources, the redistribution of noise degrades the signal-to-noise ratio of absorption features. The signal-to-noise ratio also decreases with an increased number of detectors sampling the interferogram. Because observing such spectra is a common interferometer application, the DASI has been rightly assessed (ref. 4) as having a "multiplex disadvantage" for this case.

For the case of detectors with D^*-like characteristics, the DASI signal-to-noise ratio would show the multiplex advantage but without the throughput advantage of the parallel-plate Michelson or Twyman-Green, as noted earlier.

Concluding Remarks

The digital array scanned interferometer (DASI), and other proposed equivalents, represent a new wrinkle in the long-standing contest of superiority between advocates of grating spectrometers and interferometers. The very real throughput advantage of Michelson interferometers over grating systems results from the two-dimensional acceptance angle versus resolvance inherent in Michelsons. The grating systems, on the other hand, are at a disadvantage with respect to this two-dimensional interferometer acceptance angle. The grating resolvance is inversely proportional to one of the grating acceptance angles, while the other dimension is limited by practical considerations. However, when the interferometer system is required to yield spatial as well as spectral information, the interferometer implementations have acceptance angle limitations similar to the grating system.

The Michelson can be used to realize the throughput advantage and simultaneously image by point scanning using one pixel. To do so, the system must incorporate the complexity of the spatial scanning system, which adds mechanical complexity on top of the internal mechanical scan required. The throughput factor of over 30 represents a factor of only about 6 in improved signal-to-noise ratio for photon-limited detectors. Moreover, use of an array with the grating spectrometer limits the interferometer advantage. Spatial scanning to yield the spatiospectral information further reduces the interferometer's relative performance.

The following three claims are detailed in the discussion. Michelson interferometers, which inherently have a two-dimensional acceptance angle, yield a throughput advantage. However, DASI's have no great throughput advantage over grating systems if equal spatial imaging is required of both. Therefore, this claim is not substantiated.

The flat response of the DASI's transform characteristic is real. However, the flat response is accompanied by the possibility of misinterpretation of the side lobes that result from such a response in the retrieved spectrum. In practice, interferometers often have an instrument response function that is modified to eliminate the Gibbs phenomena by apodizing or reducing the high-frequency components. Moreover, the recovered spectrum can be subjected to an attenuation function, depending on the detector size or other acceptance-angle-dependent effect that must be corrected. Thus, this claim is substantiated with reservations.

The DASI claims several other benefits, including the multiplex advantage. As shown previously, DASI has excellent performance when detecting a handful or so of monochromatic (line) sources. The signal-to-noise ratio does not decrease with increasing numbers of detectors with either photon noise or D^*-like detector noise dependence (ignoring some other noise effects that do not scale in like fashion). However, in the case of broadband sources, the transform-induced redistribution of noise punishes the signal-to-noise ratio of absorption features. A grating does not produce this undesirable effect. Therefore, with the exception of detector-noise-limited

conditions and some line-source applications, this claim is not substantiated.

As to the advantage of detection of transient events, array-based grating monochromators have this property. As to superior linearity, the high value for the low-frequency elements, i.e., the central maxima, of the interferogram would challenge the linearity of detectors more than the grating monochromator. The fall-off in higher frequency components in the interferogram may require the complexity of gain scaling to fully develop the interferogram. The claim of known and easily correctable system errors is certainly not the case in at least one of the main DASI implementations, the birefringent Wollaston interferometer. Therefore, this claim is not substantiated.

NASA Langley Research Center
Hampton, VA 23681-0001
March 6, 1996

Appendix A

Interferometer Resolution, Defocus, and Source Size Effects

The limitation on resolution for an interferometric spectrometer with finite angular subtense discussed in reference 9 forms the basis for much of the DASI's claimed advantages. For the case in this paper, the results must be modified significantly. It is useful to summarize the reference 9 results and then to develop the modified results. The case analyzed in reference 9 is that of a Twyman-Green version of the Michelson configuration. The results can be more readily illustrated with a Michelson system.

In a Michelson, the fringes are concentric rings about the optical axis. The transform scale is nonlinear, even for small angles, but is easily corrected. Placing an aperture in the focal plane of the exit lens causes a piece, or more, of a fringe to pass to a detector. As shown in reference 9, the effect is to multiply the transform by a factor:

$$F(\sigma) = \mathrm{sinc}(\sigma L n \Omega/2\pi) \tag{A1}$$

which has its first zero at $\sigma_{max} = 2\pi/L\Omega$ and where L is the mirror path length. In words, the modulation of the interferogram ceases to exist for a certain combination of solid angle and plate separation. Thus, σ must be less than some reasonable fraction of σ_{max}. On the other hand, the maximum range of the transform variable determines the ultimate resolution for the interferometer.

$$\delta\sigma = (1/l_{max})(1 - \Omega/2\pi) \tag{A2}$$

With $\Re = \sigma/\delta\sigma$, the resolvance can be written as

$$\Re = (1 - \Omega/2\pi)2\pi/\Omega \tag{A3}$$

or for a small solid angle,

$$\Re = 2\pi/\Omega \tag{A4}$$

This final result serves as the underpinning for the major claims for DASI.

For the case of Sagnac or other interferometers that produce linear parallel fringes, the finite aperture or detector subtense causes an analogous effect. Assume that the source is uniform and that the detector has an angular width $\alpha \times \beta$ in length. The signal detected will be the integrated value over the detector (ignoring the constant term that is an additional signal):

$$S(\theta) = \int_{\theta-(\alpha/2)}^{\theta+(\alpha/2)} d\theta \int d\beta \int S(\sigma, \theta)\cos[2\pi\sigma(\sin\theta)l]d\sigma \tag{A5}$$

$$S(\theta) = \alpha\beta[\sin(\pi\alpha l\sigma)/(\pi\alpha l\sigma)]\{\int S(\sigma)\cos[2\pi\sigma\sin(\theta)l]d\sigma\} \tag{A6}$$

The first zero of the sinc function is at $\sigma = 1/\alpha l$. After inversion, the spectrum will be multiplied by the sinc function, which forces the spectrum to zero at the point $\sigma = 1/\alpha l$.

There is also a maximum transform variable that, assuming θ to be small, is θl. Analogous to the Michelson case shown, the end result is to convolve the inverted interferogram with a sinc function whose first zero $1/2\theta l$ sets the ultimate resolution for the spectrum. The relationship between angle and resolvance then becomes

$$\begin{aligned} \Re &= 2\theta l\sigma \\ &= 2\theta l/\alpha l \end{aligned} \tag{A7}$$

or, with θ no larger than $\pi/2$, becomes

$$\Re = \pi/\alpha \tag{A8}$$

Picking up the β dimension, the results for the acceptance angle versus resolution are

$$\Omega = \alpha\beta$$
$$= \pi\beta/\Re \tag{A9}$$

and for the étendue results are

$$A\Omega = \pi\alpha\beta A \tag{A10}$$

$$A\Omega = \pi A\beta/\Re \tag{A11}$$

This final very important result shows that modifying the interferometer to have parallel fringes by using a Sagnac with fringes localized at infinity, with a Michelson with wedged mirrors with fringes localized in the wedge, or a Wollaston polarization interferometer produces the same effect: The acceptance angle is inverse to the resolvance.

Defocus Effects

In a Michelson interferometer with tilted mirrors, which gives a set of linear fringes, a defect of focus causes a limitation on spectral resolution with increased aperture. As shown in figure A1, mirrors M1 and M2 tilted at angle Θ would have fringes localized at the surface of M2 for on-axis rays that represent a point source on the axis. If the source is extended to an angular dimension Ψ, the source half-angle, then the reflected ray pair seems to come from a common point that is offset in ΔX and ΔY as shown. The following equations determine the offset values:

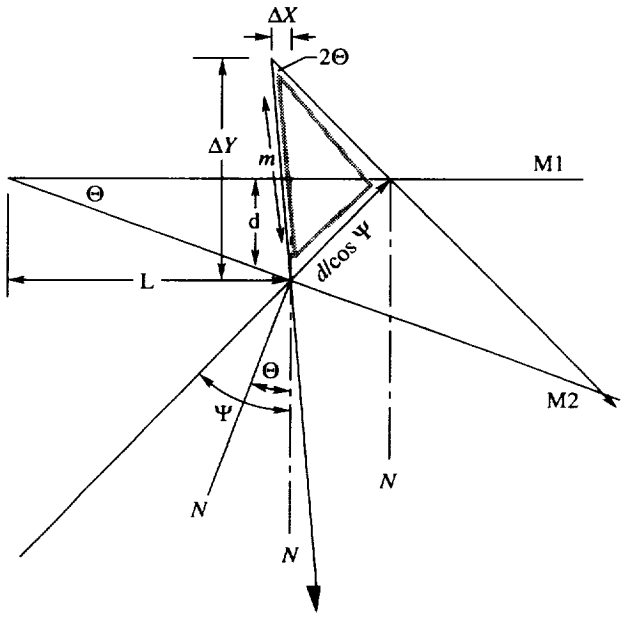

Figure A1. Definitions of defocus for air wedge interferometer.

$$d = \mathrm{L}\tan\Theta \tag{A12}$$

$$m/\sin(180 - 2\Psi) = (d/\cos\Psi)/\sin 2\Theta \tag{A13}$$

From the shaded triangle in figure A1,

$$\Delta Y = m\cos(\Psi - 2\Theta) \tag{A14}$$

$$\Delta X = m\sin(\Psi - 2\Theta) \tag{A15}$$

From these equations, we can solve for ΔX and ΔY in terms of L (the interferogram length from the mirror apex), Θ, and Ψ, giving

$$\left.\begin{aligned} \Delta X &= L \tan\Theta \csc 2\Theta \sec\Psi \sin 2\Psi \sin(\Psi - 2\Theta) \\ \Delta Y &= L \tan\Theta \csc 2\Theta \sec\Psi \sin 2\Psi \cos(\Psi - 2\Theta) \end{aligned}\right\} \tag{A16}$$

Using the small angle approximation:

$$\left.\begin{aligned} \Delta X &= L\Psi^2 \\ \Delta Y &= L\Psi \end{aligned}\right\} \tag{A17}$$

From the preceding equations, one can see that the greatest delta error is ΔY, but this finding is somewhat misleading. The ΔY or the defocus term is not, in itself, the critical factor but rather the blur diameter in the focus plane M2 that results from the defocus. This diameter is the defocus times the apex angle 2Θ, giving

$$\text{Blur diameter due to defocus} = 2L\Psi\Theta = \Delta X_{\text{sample}} \tag{A18}$$

The blur diameter in turn sets the sample interval ΔX_{sample} and detector size in a detector array (along with the diffraction and geometric blurs of the optics which are ignored here). The sample interval and the total length of a two-sided interferogram L_0 are related to the spectral resolution $\Re$ by

$$\Re = L_0/\Delta X_{\text{sample}} = 1/2\Psi\Theta \quad (L_0 = L) \tag{A19}$$

Then the allowable source subtense is proportional to the inverse of the spectral resolution:

$$\Psi \propto 1/\Re \tag{A20}$$

Laterally Displaced Source and Acceptance Angle Limitations

A fixed source splitting (laterally displaced) in a Sagnac or wedged Twyman-Green coupled with increasing source size causes an effect at the detector plane equivalent to integrating over the detector acceptance angle. This effect comes from a source width phase shift in the collimated light reaching the detector plane. The separation of the coherent twinned rays yields the interferogram as expected, but contributions from distributed pairs across the source incur additional phase shift from the increasing total path length to a particular point on the detector plane. This phenomenon, essentially an obliquity effect, causes the "phase zero" of the interferogram to shift linearly with increasing acceptance angle.

For a lateral displacement interferometer, such as the Sagnac, the effects of an increasing source subtense can be calculated. The apparent source displacement distance d and the source size D can be related to the angles between the plane waves (Θ and Θ') exiting from the monochromator collimating lens, as shown in figure A2. Using the summation of two plane waves, E_1 and E_2, the intensity of the interferogram I is

$$I = (E_1 + E_2)(E_1 + E_2)^* \tag{A21}$$

where $E = A_0 e^{ik'r'}$ vector intensity is

$$\begin{aligned} I = 2A_0^2\{1 + \cos[k(xi_x + yi_y)][(\cos\Theta i_x + \sin\Theta i_y) \\ - (\cos\Theta' i_x + \sin\Theta' i_y)]\} \end{aligned} \tag{A22}$$

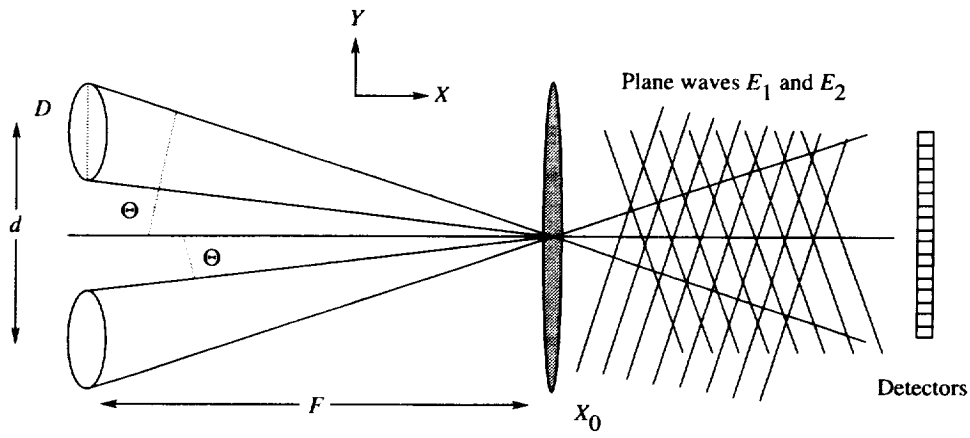

Figure A2. Definitions of aperture function calculation.

and where, from figure A2 and other substitutions

$$\Theta = \tan^{-1}[D-(d/2)]/F \approx [D-(d/2)]/F \tag{A23a}$$

$$\Theta = \tan^{-1}[D+(d/2)]/F \approx [D+(d/2)]/F \tag{A23b}$$

$$k = 2\pi\sigma \tag{A24}$$

$$\cos\Theta - \cos\Theta' \approx (\Theta'^2 - \Theta^2)/2 = Dd/F^2 \tag{A25a}$$

$$\sin\Theta - \sin\Theta' \approx (\Theta - \Theta') = -d/F \tag{A25b}$$

Integrating over the source size D from zero to D_0 and fixing x at the detector plane distance X_0, we get

$$I_{(x,y)} = 2A_0 + 2A_0\int\cos[(kDd/F^2)x - (kd/F)y]\delta D \tag{A26}$$

$$I_{(D_0,X_0,y)} = 2A_0D_0\{(1+\mathrm{sinc}(D_0dkX_0/2F^2) \times \cos[(kd/2F^2)(-D_0X_0+2Fy)]\} \tag{A27}$$

The preceding equation states that the interferogram is limited by a sinc function that is dependent on not only the source apparent displacement but also the source size. The first zero is at $D_0 = F^2/\sigma dX_0$ or, in angular terms, $\Theta_s = F/\sigma dX_0$. If $X_0 \approx 2F$, the zero of the sinc function can be written as $\sigma_{max} = 1/(2\Theta_s d)$, and the source subtense limits the interferogram visibility and maximum upper usable wave number. The sinc function plays a role similar to the finite aperture of the detector elements thereby causing a linear inverse relationship between acceptance angle and resolvance $\Re$.

Appendix B

Signal-to-Noise Relationships

The multiplex advantage for Sagnac and Wollaston prism versions of DASI's can, in reality, be thought of as disadvantages when compared with moveable mirror interferometers or grating instruments. This rationale results from the fact that the DASI's share the incoming radiation with all the N elemental detectors. The signal-to-noise ratio can then be recovered in the inversion process because the signal to noise will increase. However, it increases only as the square root of the number of detectors. If the signal drops below the detector-amplifier inherent noise and away from the photon-noise limit, the residual influence of the nonphoton noise more or less punishes the recovery of the signal-to-noise ratio.

In view of that information, the results from Kahn now can be applied to show that the transform instruments *may or may not* have an advantage over sequential grating instruments. As noted in reference 12, in the photon-noise-dominated regime, the sequential transform instrument has no general advantage over a sequentially scanned grating instrument, all other things being equal, including throughput. Spectra with great fluctuation (over twice the average value) favor the transform instrument, whereas more benign spectra favor the grating instrument.

For detector array grating instruments, the results of Kahn (ref. 12) indicate that the grating instruments would be superior to sequentially transform instruments by the square root of the number of samples in the imaging cases of interest here. This result amplifies the comment in reference 4 concerning the multiplex disadvantage of DASI's, which had been at odds with other claims for a multiplex *advantage.*

The relationship of noise generated during the data-taking process was presented in Kahn (ref. 12), but it is worth deriving this result in the array case. Assume that the detectors are in the photon-noise-limited case, yielding Poisson noise uncorrelated detector to detector. The detection process consists of integrating generated charges arising from incident photons. The signal-generating process can be written as having an average value and a standard deviation around that mean.

With unity quantum efficiency and in unit time, write the detected signal charge as

$$S(K) = \int_0^\infty S(\sigma)[1 + \cos(2\pi K\sigma)]d\sigma \tag{B1}$$

The inversion process involves multiplying by cosines of various frequencies, summing over the frequency sample points, and scaling:

$$S'(\sigma) = \sum_{K=0}^{K=K_{max}} S(K)\cos(2\pi K\sigma) \tag{B2}$$

Inserting the expression for the transformed spectrum gives

$$S'(\sigma) = \sum_{K=0}^{K=K_{max}} \int_0^\infty S(\mu)[1 + \cos(2\pi K\mu)]d\mu\cos(2\pi K\sigma) \tag{B3}$$

$$S'(\sigma) = \int_0^\infty S(\mu)1/2\sum\{\cos[2\pi K(\mu + \sigma)] + \cos[2\pi K(\mu - \sigma)]\}d\mu \tag{B4}$$

Rearranging and using the relation

$$1 + x + x^2 + x^3 + \ldots + x^n = (1 - x^n)/(1 - x)$$

gives

$$S'(\sigma) = 1/2\Big(\int_0^\infty d\mu\ S(\mu)\{\cos[\pi N\delta k(\mu-\sigma)] \times \sin[\pi\delta k(N+1)(\mu-\sigma)]/\sin[\pi\delta k(\mu-\sigma)]\} + \text{Equivalent function of } (\mu+\sigma)\Big) \tag{B5}$$

where K_{max} is now N, the number of transform samples, times the smallest interval δk.

If N is reasonably large, the integrand exists only around $\sigma = \mu$, scaled by the peak value of the $(\sin x)/x$ term $(N + 1)$ and within a width of $1/\delta k(N + 1)$.

$$S'(\sigma) = (1/2\delta k)S(\sigma)$$

Thus, the inversion process gives the input spectrum, modified by a scale factor of $(1/2\delta k)$. The constant term in the interferogram yields a similar term, except that it exists for $\sigma = 0$ and has a value equal to the integral of the spectrum over all wave numbers. This term is also a constant. Note that this term represents the average value for the spectrum and has the effect of generating noise.

Under the assumption that the detector noise is a Poisson process, as would be the case for photon-noise-limited performance, the noise can be calculated. The analysis can be simplified by noting that the noise in any element of the sampled spectrum is assumed to be independent from the other spectrum elements. Thus, when calculating the variance, only signals from the same spectral element contribute:

$$\langle S_n^2(\sigma)\rangle = (\mathrm{SF})^2\langle\sum\sum S(k)S(k')\cos(2\pi k\sigma)\cos(2\pi k'\sigma)\rangle \tag{B6}$$

$$\langle S_n^2(\sigma)\rangle = (\mathrm{SF})^2\sum S(k)\cos^2(2\pi k\sigma) \tag{B7}$$

Inserting for $S(k)$ and remembering to carry the constant term because it represents the background signal results in

$$\langle S_n^2(\sigma)\rangle = (\mathrm{SF})^2\sum\left\{\int_0^\infty S(\mu)[1+\cos(2\pi k\mu)]d\mu\right\}\cos^2(2\pi k\sigma) \tag{B8}$$

Expanding the integral and expressing the cosine products as sum and difference frequencies, as done in equation (B8), yields

$$\langle S_n^2(\sigma)\rangle = 2N\delta k^2\int d\mu S(\mu) + 2\delta k^2\Big[\int d\mu S(\mu)\Big]\Delta(\sigma) + \delta kS(0) + [\delta kS(2\sigma)/2] + [\delta kS(-2\sigma)/2] \tag{B9}$$

where $\Delta(\sigma)$ is a delta function around zero wave number (dc). The term affecting the reconstructed spectrum is the first and gives a root mean squared (RMS) of

$$\langle S_n^2(\sigma)\rangle^{1/2} = (2N)^{1/2}\delta k\Big[\int d\mu S(\mu)\Big]^{1/2} \tag{B10}$$

Multiplying and dividing by the effective wave-number interval $\Delta\sigma$ in the integrand allows the noise to be expressed with respect to an average spectrum:

$$\langle S_n^2(\sigma)\rangle^{1/2} = 2^{1/2}S_{avg}^{1/2}N^{1/2}\delta k\Delta\sigma^{1/2} \tag{B11}$$

Remember that $N\delta k$ is the wave-number span whose reciprocal is the minimum resolution interval $\delta\sigma$. Therefore, the signal-to-noise ratio can be written:

$$S(\sigma)/\langle Sn^2(\sigma)\rangle^{1/2} = S(\sigma)\delta\sigma/\sqrt{2S_{avg}\Delta\sigma/N} \tag{B12}$$

Noting that the highest value for $\Delta\sigma$ is $1/\delta k$ and for $\delta\sigma$ is $1/N\delta k$, the final result is obtained:

$$S/N = S(\sigma)\delta\sigma/\sqrt{2S_{avg}\delta\sigma} \tag{B13}$$

Three cases follow to illustrate these results: (1) a monochromatic source, such as a laser, (2) a broadband source typical of black bodies either viewed directly or in reflection, and (3) a detector-noise-limited case.

Monochromatic Source

Let $S(\sigma) = U_0(\sigma_0)$ with $\sigma_0 < \sigma_{max}$. Then the transform can be written:

$$S(k_i) = \Delta\{[\cos(2\pi k_i\sigma_0)\sin(\pi\Delta\sigma_0)/\pi\Delta\sigma_0] + 1\} \tag{B14}$$

Invert by using

$$S(\sigma) = 2\delta k \sum_{k_i=0}^{k_{max}} S(k_i)\cos(2\pi k_i\sigma)$$

With $k_{max} = N\delta k$, the detector subtended angle Δ, and $k_i = i\delta k$, the inversion can be written:

$$\begin{aligned} S(\sigma) = 2\delta k\Delta\Big(\sum 1/2\{&\cos[2\pi i\delta k(\sigma - \sigma_0)] \\ &+ \cos[2\pi i\delta k(\sigma + \sigma_0)]\} \\ &+ \sum\cos(2\pi i\delta k\sigma)\Big) \end{aligned} \tag{B15}$$

$$\begin{aligned} S(\sigma) = 2\delta k\Delta(\{&\cos[\pi N\delta k(\sigma - \sigma_0)]\sin[\pi\delta k(N+1)(\sigma - \sigma_0)]/\sin[\pi\delta k(\sigma - \sigma_0)]\} \\ &+ \text{Equivalent function of } (\sigma + \sigma_0)) \end{aligned} \tag{B16}$$

At $\sigma = \sigma_0$, $S(\sigma) = (N + 1)\delta k\Delta$ and has a full width of $1/(N\delta k)$ defined by first zeros of the function. The area of the function is approximately Δ from the height-width product equivalent to the unit area of the delta function monochromatic source, but reduced by the detector angular subtense.

The signal-to-noise ratio from equation (B13) is

$$\begin{aligned} S/N &= (N + 1)\delta k\delta\sigma^{1/2} \\ &= 1/(2\delta\sigma)^{1/2} \end{aligned} \tag{B17}$$

From this result, it appears that a monochromatic source has a signal-to-noise ratio that is independent of the angular subtense of the individual detectors.

Broadband Source

Assuming that a broadband source signal-to-noise characteristic can be illustrated by a constant value of spectral irradiance, the result from equation (B13) can be used to yield

$$S/N = \Delta S_0/[2^{1/2}(S_0\Delta\sigma_{max})^{1/2}N^{1/2}\delta k] \tag{B18}$$

Because $\int_0^\infty S_0 \delta\sigma/\sigma_{max} = S_0$ (after identifying Δ as δk), equation (B18) can be simplified:

$$S/N = \Delta S_0/[2^{1/2}(S_0\Delta)^{1/2}N^{1/2}\delta k^{1/2}]$$
$$= S_0\Delta^{1/2}(2S_0N\delta k)^{1/2} \quad \text{(B19)}$$

$$S/N = S_0(\Delta N\delta k)^{1/2}/[2(S_0)^{1/2}N\delta k]$$
$$= S_0\delta k\delta\sigma/(2S_0\delta\sigma\delta k)^{1/2} \quad \text{(B20)}$$

Detector-Noise-Limited Case

Let the dominant noise source be from the photodetector, and let the photodetector have a noise proportional to its area. Such a detector will have a noise charge of $n_0 = n_0{}^*(\delta k)^{1/2}$, which is dependent only on the square root of its area. It is assumed that the length of the detector can be made as long as necessary and does not vary as the acceptance angle δk is varied. Under these conditions, the signal-to-noise ratio can be written:

$$S/N = S(\sigma)\Delta/(2N)^{1/2}\delta k n_0$$
$$= S(\sigma)\Delta/(2^{1/2}n_0\delta kN/N^{1/2})$$
$$= S(\sigma)\Delta/[2^{1/2}n_0{}^*\delta k^{1/2}/(N^{1/2}\delta\sigma)]$$
$$= S(\sigma)\Delta\delta\sigma/(2n_0{}^{*2}\delta k^2/N\delta k)^{1/2} \quad \text{(B21)}$$

or with $\Delta = \delta k$,

$$S/N = S(\sigma)\delta\sigma/(2n_0{}^{*2}\delta\sigma)^{1/2} \quad \text{(B22)}$$

Therefore, the signal-to-noise ratio is independent of the number of detectors or detector angular subtense, as long as the minimum resolution $\delta\sigma = (N + 1)\delta k$ remains constant.

References

1. Hammer, P. D.; Valero, F. P. J.; Peterson, D. L.; and Smith, W. H.: Remote Sensing of Earth's Atmosphere and Surface Using a Digital Array Scanned Interferometer—A New Type of Imaging Spectrometer. *J. Imaging Sci. & Technol.*, vol. 36, issue 5, Sept.–Oct. 1992, pp. 417–422.

2. Smith, W. H.: unpublished article submitted to *Exp. Astron.*, April 1993.

3. Hammer, Philip D.; Valero, Francisco P. J.; Peterson, David L.; and Smith, William Hayden: An Imaging Interferometer for Terrestrial Remote Sensing. *SPIE OE/Aerospace Sensing 1993*, Sept. 1993, pp. 244–255.

4. Smith, Wm. Hayden; and Schempp, W. V.: Digital Array Scanned Interferometers for Astronomy. *Exp. Astron.*, vol. 1, no. 6, 1990–1991, pp. 389–405.

5. Okamoto, T.; Kawata, S.; and Minami, S.: Fourier Transform Spectrometer With a Self-Scanning Photodiode Array. *Appl. Opt.*, vol. 23, Jan. 1984, pp. 269–273.

6. Aryamanya-Mugisha, Henry; and Williams, Ronald R.: A Fourier Transform Diode Array Spectrometer for the UV, Visible, and Near-IR. *Appl. Spectrosc.*, vol. 39, no. 4, 1985, pp. 693–697.

7. Jacquinot, Pierre: The Luminosity of Spectrometers With Prisms, Gratings, or Fabry-Perot Etalons. *J. Opt. Soc. America*, vol. 44, no. 10, Oct. 1954, pp. 761–765.

8. Born, Max; and Wolf, Emil: *Principles of Optics*, Second revis. ed. Macmillan Co., 1964.

9. Vanasse, George A.; and Sakai, Hajime: Fourier Spectroscopy. *Progress in Optics—Volume VI*, E. Wolf, ed., North Holland Publ. Co., 1967, pp. 261–330.

10. Jacquinot, P.: New Developments in Interference Spectroscopy. *Rep. Prog. Phys.*, vol. 23, 1960, pp. 267–312.

11. Fellgett, P. J.: A Contribution to the Theory of Multiplex Interferometric Spectrometry, *J. de Phys. et Radium*, vol. 19, 1958, p. 187.

12. Kahn, F. D.: The Signal-Noise Ratio of a Suggested Spectral Analyzer. *Astrophys. J.*, vol. 129, no. 2, Mar. 1959, pp. 518–521.

REPORT DOCUMENTATION PAGE

Form Approved
OMB No. 0704-0188

1. AGENCY USE ONLY *(Leave blank)*	2. REPORT DATE	3. REPORT TYPE AND DATES COVERED
	August 1996	Technical Paper

4. TITLE AND SUBTITLE
Performance Assessment of the Digital Array Scanned Interferometer (DASI) Concept

5. FUNDING NUMBERS
WU 225-89-00-01

6. AUTHOR(S)
Stephen J. Katzberg and Richard B. Statham

7. PERFORMING ORGANIZATION NAME(S) AND ADDRESS(ES)
NASA Langley Research Center
Hampton, VA 23681-0001

8. PERFORMING ORGANIZATION REPORT NUMBER
L-17480

9. SPONSORING/MONITORING AGENCY NAME(S) AND ADDRESS(ES)
National Aeronautics and Space Administration
Washington, DC 20546-0001

10. SPONSORING/MONITORING AGENCY REPORT NUMBER
NASA TP-3570

11. SUPPLEMENTARY NOTES
Katzberg: Langley Research Center, Hampton, VA; Statham: Lockheed Martin Engineering & Sciences Company, Hampton, VA.

12a. DISTRIBUTION/AVAILABILITY STATEMENT
Unclassified–Unlimited
Subject Category 35
Availability: NASA CASI (301) 621-0390

12b. DISTRIBUTION CODE

13. ABSTRACT *(Maximum 200 words)*
Interferometers are known to have higher throughput than grating spectrometers for the same resolvance. The digital array scanned interferometer (DASI) has been proposed as an instrument that can capitalize on the superior throughput of the interferometer and, simultaneously, be adapted to imaging. The DASI is not the first implementation of the dual purpose concept, but it is one that has made several claims of major performance superiority, and it has been developed into a complete instrument. This paper reviews the DASI concept, summarizes its claims, and gives an assessment of how well the claims are justified. It is shown that the claims of signal-to-noise ratio superiority and operational simplicity are realized only modestly, if at all.

14. SUBJECT TERMS	15. NUMBER OF PAGES
Interferometer; Imaging; Multispectral imager throughput; Signal to noise	26
	16. PRICE CODE: A03

17. SECURITY CLASSIFICATION OF REPORT	18. SECURITY CLASSIFICATION OF THIS PAGE	19. SECURITY CLASSIFICATION OF ABSTRACT	20. LIMITATION OF ABSTRACT
Unclassified	Unclassified	Unclassified	